Regular Article

Time-resolved photoluminescence imaging for the mapping of weakly luminescent pigments in paintings

Marta Ghirardello[1,a] **, Alessia Candeo**[1]**, Benedetto Ardini**[1]**, Gianluca Valentini**[1]**, Cristian Manzoni**[2]**, Thomas Calligaro**[3]**, Laurent Pichon**[3]**, Xueshi Bai**[3]**, Roland Lenz**[4]**, Roberto Alberti**[5]**, Michele Gironda**[5]**, Daniela Comelli**[1]

[1] Department of Physics, Politecnico di Milano, Piazza Leonardo da Vinci 32, Milan, Italy
[2] CNR-IFN, Piazza Leonardo da Vinci 32, Milan, Italy
[3] Centre de Recherche et de Restauration des Musées de France (C2RMF), Palais du Louvre, Paris, France
[4] Institute for Conservation Sciences, Staatliche Akademie Der Bildenden Künste, Am Weißenhof 1, Stuttgart, Germany
[5] XGLab S.R.L.-Bruker Nano Analytics, Via Conte Rosso 23, Milan, Italy

Abstract UV–Vis-induced luminescence techniques are commonly employed by conservators and restorers to examine cultural heritage objects in a non-invasive manner. Many chemical components in artworks show luminescent emission, which can be used for both diagnostic and conservative purposes. The emission spectrum and lifetime are precious indicators of the fluorophore nature and the combination of these information enhance the analytical power of the technique. In this work, we propose the combined application of photoluminescence lifetime imaging and time-gated hyperspectral imaging to estimate the lifetime of the emitters and reconstruct their spectral emission at the different timescales in paintings. The combination of these techniques allows the in-depth characterization of the emission properties of luminescent materials, further providing their spatial distribution in the analysed area. The approach was initially assessed on different model paints to identify and characterize which show optical emission, and subsequently, on different historical paintings. Therein, we demonstrate how the time-resolved imaging approach is highly effective for the identification and mapping of weak luminescent pigments in artworks. In particular, we show how the faint emission from lead white paints can be detected by exploiting its long-living emission (with a lifetime of hundreds of microseconds), despite the presence of other strongly fluorescent materials such as varnish, binders and brightly emitting luminescent pigments.

1 Introduction

In recent years, the development of characterization techniques based on optics and photonics has increased considerably, leading to both the improvement of existing techniques and to the development of new technologies, some of which have been also exploited for the scientific analysis of cultural heritage (CH). For example, Daffara and co-authors [1] demonstrated the capabilities of optical profilometry based on scanning conoscopic holography to retrieve with high-resolution and high-accuracy the micro-structured surface of highly reflective metal artworks. In Dal Fovo et al. [2], it is shown how photoacoustic imaging can be employed to uncover hidden features and provide structural information in multi-layered objects. Optical-photothermal infrared (O-PTIR) spectroscopy [3] is a recently developed technique that provides infrared (IR) spectra with nanometric spatial resolution, pushing the boundaries of the traditional—and widely employed in the CH field—molecular spectroscopy. Brillouin light scattering [4], a powerful analytical tool in condensed matter physics and material science, has been applied for the study of the elastic and viscoelastic properties of oil paints, exploiting the inelastic scattering of light from thermally activated acoustic waves. These are only some of the examples showing how optical and photonic techniques have been recently applied to CH to provide chemical, structural and morphological information of artworks in a non-invasive and non-destructive way.

In this context, UV–Vis-NIR spectroscopy and imaging are well-established photonics techniques for the non-invasive study of artworks [5]. Diffused reflectance spectroscopy is commonly applied [6] in both point-like (as fibre optic reflectance spectroscopy, FORS [7]) and imaging modality [8], allowing the identification of colourants and pigments in paintings and other polychromatic artistic surfaces, especially when the method is applied in a broad spectral range, which can extend to the short-wave infrared or mid-infrared [9]. UV–Vis-induced luminescence spectroscopy can be applied for the non-invasive identification and mapping of luminescent compounds through their characteristic emissions [10–13], supporting the classification obtained with elemental and molecular analyses. Nonetheless, photoluminescence (PL) spectroscopy and imaging are less widely employed than reflectance techniques in CH. Their relative limited use can be related to the challenging and misleading interpretations of the emission spectrum.

[a] e-mail: marta.ghirardello@polimi.it (corresponding author)

Indeed, due to the superimposition of the emission from different species, intrinsic similarities in the emission spectra of different fluorophores [14–16] and effect of reabsorption or scattering effects ascribed to paint composition [17–20], the interpretation of the emission spectrum is not straightforward. Besides, when using continuous excitation and detection schemes, only the most intensely emitting materials (typically protective varnish and organic compounds) can be detected, while weaker emissions are usually masked.

Despite these limits, PL is a very sensitive technique that allows one to detect trace amounts of luminescent compounds [11] when present in a non-emitting background. Time-resolved PL measurements can improve the specificity with respect to steady-state PL measurements by resolving the decay dynamics of the emissions and separating the emissions occurring at different timescales. Time-correlated single photon counting devices, with picoseconds resolution and applied in point like mode, were used to retrieve the decay kinetic of selected points of CH materials and objects either in laboratory [16, 20] or in situ [21]. Time-resolved systems relying on the use of a time-gated intensified camera were also developed to investigate the emission lifetime of artworks with different temporal resolution, ranging from nanosecond [22–25] to microsecond timescale [26–28]. However, since the emission decay depends on radiative and non-radiative de-excitation processes, which are highly influenced by the interaction of the fluorophore with its microenvironment, the emission lifetime cannot be considered as an absolute value to identify an emitting material. Nonetheless, by combining the temporal information with the spectral one it is possible to gain further insight in the PL process. This approach has proven particularly effective in the analysis of modern paintings that contain luminescent materials with different lifetimes [26, 29].

Here, we propose the combined use of two time-resolved imaging methods to detect and identify weakly emitting materials in paintings. The approach consists of using in a first step a PL lifetime imaging camera to identify the order of magnitude of the lifetimes of the emission present in the analysed painted surface, and then to use a time-gated hyperspectral imaging (HSI) system to reconstruct the emission spectrum of the materials emitting in each different timescale of interest (Fig. 1). The comprehensive characterization of the emission properties of luminescent materials on the surface of an artwork allows to identify such materials even in the presence of multiple emitting species. Illustrative examples of the proposed approach will be presented, including results obtained from reference materials, model and historical paintings.

2 Materials and methods

2.1 Materials

As a first test, different model paints were measured to identify those showing luminescent emission. The model paints were prepared by bounding pigments with Tylose MH 300 5% in water (Kremer Pigments) or pre-polymerized linseed oil (Zecchi) and then by applying them on a plywood prepared with a ground of calcium carbonate (Kremer Pigmente). The complete list of pigments is reported in Table S1 in Supporting Information (SI). All model paints were first characterized with time-resolved photoluminescence (TRPL) spectroscopy and then analysed with the PL imaging protocol, combining lifetime imaging and time-gated hyperspectral imaging.

The PL imaging protocol was then applied on a model painting and on two historical paintings (Fig. S1). The model painting (40×65 mm), depicting a blue draped cloth, was painted 35 years ago with traditional pigments bound in an egg-based binding medium over a wooden panel with a gypsum ($CaSO_4$) ground preparation. The historical paintings are the modern painting *Madre* by Pietro Verzetti (1918, oil paint on canvas, 105×125 cm, Accademia di Brera, Milano, Italy) and the Renaissance painting *Christ en croix et Saintes Femmes* by Albrecht Altdorfer (around 1520, oil paint on wood, 59.5×44.5 cm, Musée de l'Œuvre Notre-Dame, Strasbourg, France, inventory number: 22.995.0.661.1).

2.2 Methods

In this research, we employed three time-resolved setups sensitive to the transient decay kinetic of luminescent materials: a time-resolved PL spectrometer, a lifetime imaging system and a time-gated HSI system. The first setup was used for preliminary investigations, aimed at assessing the emission properties (spectrum and lifetime) of reference luminescent pigments. The latter two set-ups were used to analyse model and historical paintings and assess how their combined use allows the identification and mapping of luminescent materials. Details on the three setups are provided in the following paragraphs. Here, we remark that the three setups employ the same nanosecond pulsed laser source – to excite the transient decay kinetic of luminescent materials – and the same time-gated intensified camera – to temporally sampling the transient decay kinetic of PL emissions.

2.2.1 Time-resolved photoluminescence (TRPL) spectroscopy

Time-resolved photoluminescence (TRPL) spectroscopy was performed on model paints to characterize their emission spectrum and decay kinetic. The system, fully described in Artesani et al. [28], records a sequence of time-gated PL spectra at different delays with respect to the laser pulses. The laser light (third harmonic of Nd:YAG Q-switched laser, FTSS 355–50 CryLas GmbH, $\lambda = 355$ nm,
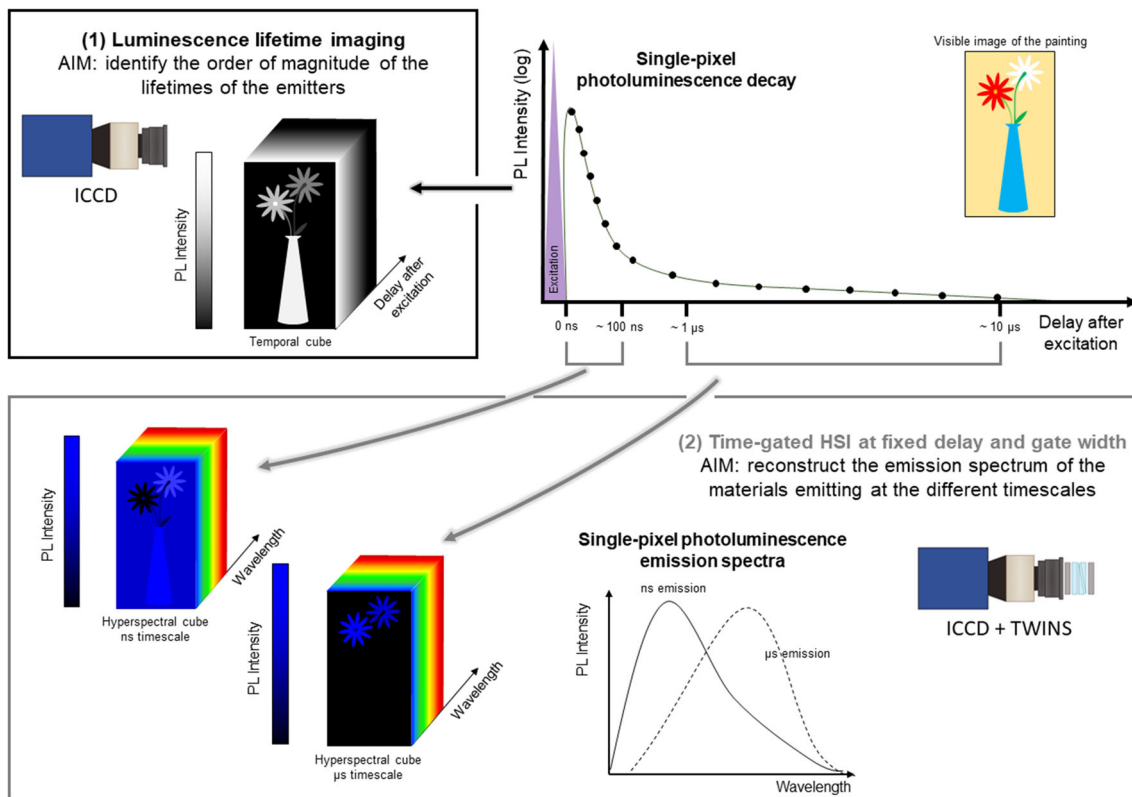
Fig. 1 Scheme of the PL decay of a single pixel of the image of the painting showing pulsed laser excitation (purple), PL emission (grey line), PL decay kinetic sampling (black circles) and time-gated PL measurements (grey square brackets). Initially, PL lifetime imaging is performed to identify the order of magnitude of the emission (top panel, left). This is done by sampling the decay (black circles) at different delays with respect to pulsed excitation and reconstructing the decay kinetic of each image pixel through a time-gated intensified camera. In this way, it is possible to create temporal cubes in which each pixel contains the information of the decay of the PL emission. Once the order of magnitude of the lifetime of the emission has been identified, time-gated HSI is performed by fixing the delay and the temporal window of the time-gated camera and recording a hyperspectral datacube in that temporal window (bottom panel). This results in hyperspectral cubes in which each pixel contains the time-gated emission spectrum of the analysed area

1.0 ns pulse, 100 Hz repetition rate) is coupled to a multimode silica fibre (600 μm core) and, through a proper optical system, illuminates a spot on the sample surface of 1 mm diameter. The PL emission from sample is collected in a backscattering geometry and focused into the entrance slit of an imaging spectrometer (Acton Research 2300i) coupled with a time-gated intensified camera (C9546-03, Hamamatsu Photonics and Retiga R6, Qimaging). The latter device allows photons to be detected in a time window of any duration between 3 ns to 1 ms. A custom-built trigger unit and a precision delay generator (DG535, Stanford Research System) complete the whole system, which has an overall temporal jitter close to 500 ps. The system can be employed to detect the emission spectrum in a selected temporal window (giving rise to the so-called time-gated spectrum) or to measure the emission decay kinetic at different wavelengths. In the latter case, a multiexponential decay with a maximum of three components was used to fit the kinetic data integrated over a selected spectral region of interest, using a nonlinear least-squares fitting methods [28]. The effective lifetime was then calculated as the average of the lifetimes weighted over the number of photons originating from each decay path, following the equation $\tau_{\mathrm{eff}} = \frac{\sum_i A_i \tau_i^2}{\sum_i A_i}$, where A_i and τ_i refer to the amplitude and lifetime of each component of the multi-exponential decay model.

2.2.2 Luminescence Lifetime Imaging

Luminescence lifetime imaging was performed to estimate the lifetime of the emitters present in the analysed samples and paintings with a portable system, fully described in Nevin et al. [30], which here is briefly summarized. The apparatus is comprised the pulsed nanosecond laser excitation source ($\lambda = 355$ nm, 1.0 ns pulse) described in the previous TRPL setup combined with the time-gated intensified camera. A custom-built trigger unit and the precision delay generator complete the system.

The laser beam is coupled to a silica optical fibre, whose fibre tip is magnified with suitable optics to uniformly illuminate a circular area of about 25 cm in diameter of the surface under analysis. The PL emitted by the illuminated surface is imaged by the time-gated camera through a high-aperture photographic camera lens (Nikon Nikkor, f = 50 mm, F/# = 1.2).

The PL decay is temporally sampled by the time-gated camera, whose temporal window is adjustable from 3 ns to 1 ms, depending on the kinetic properties of the surface under investigation. In this research, we investigated the PL decay kinetics occurring at three different timescales, in the following quoted as nanosecond, microsecond and millisecond decay kinetics. Typical measurement parameters used are the following:

(i) *nanosecond timescale:* PL decay kinetic is sampled from 0 to 50 ns after excitation with 1 ns sampling step and a temporal window of 10 ns;

(ii) *microsecond timescale*: PL decay kinetic is sampled from 0.2 to 100 μs with a sampling step of 10 μs and a temporal window of 10 μs;

(iii) *millisecond timescale*: PL decay kinetic is sampled from 0.1 to 5 ms with a sampling step of 0.1 ms and a temporal window of 100 μs.

Typically, the acquisition time for an entire luminescence lifetime imaging dataset is below 5 min. The lifetime map is calculated pixel-by-pixel by modelling the emission decays with a mono-exponential model and is then displayed in a false colour representation [31].

2.2.3 Time-gated Hyperspectral Imaging (TG-HSI)

Time-gated Hyperspectral Imaging (TG-HSI) was employed to reconstruct hyperspectral datacubes of the PL emission from paintings in different timescales of interest, previously identified through the lifetime imaging setup. A detailed description of the system is reported in Ghirardello et al. [29]. PL excitation is provided again by the Q-switched Nd:YAG pulsed laser ($\lambda = 355$ nm, 1.0 ns pulse), whose laser beam is enlarged through optics to illuminate a portion of the surface to be analysed of 10 cm in diameter size. To collect PL spectral images of the surface under analysis, a common-path birefringent interferometer is placed in front of the time-gated intensified camera, while synchronization between illumination and detection is provided by the precision delay generator and a custom-built trigger unit described previously.

The interferometer allows one to obtain high-quality interferograms for each point of the field of view. By means of the Fourier transform, the interferograms are converted to high-quality spectra, reconstructed in the spectral range where the time-gated camera is sensitive (370–850 nm) with a maximum spectral resolution of 4 nm at 600 nm wavelength.

The acquisition protocol consisted of recording time-gated hyperspectral datacubes of the PL emission occurring at fixed delays after excitation. Typical parameters were:

(i) *nanosecond timescale:* temporal window of 100 ns synchronous with the laser excitation;

(ii) *microsecond timescale*: temporal window of 10 μs delayed by 0.15 μs with respect to the pulsed excitation;

(iii) *millisecond timescale*: temporal window of 0.1 ms delayed by 50 μs with respect to the pulsed excitation.

The acquisition time for each spectral datacube was in the order of 10 min for the nanosecond timescale and 30–45 min for the microsecond/millisecond timescales. Data analysis includes the extraction of spectral images and their combination in a false colour representation as well as the extraction of PL emission spectra in selected regions of interest (ROIs) of the analysed surface.

2.2.4 X-ray fluorescence (XRF) mapping

Two scanning MA-XRF systems were employed to achieve the spatial distribution of the chemical elements in the analysed paintings and to confirm the identification of luminescent materials provided by the time-resolved PL imaging protocol.

XRF maps of Altdorfer's painting were acquired with the MA-XRF system developed at the C2RMF and described in Ravaud et al. [32]. The head of the system, with a collimated Mo X-ray generator (40 kV, 0.6 mA) and a fast SDD X-ray detector (50 mm^2), was raster scanned in front of the painting in two scan for a total area of 45.5 cm $\times$ 61.0 cm, with a 1-mm step size and 10 ms dwell time per pixel. The model painting and the painting *Madre* were mapped with the commercial Bruker CRONO. The detailed description of the system is reported in Alberti et al. [33]. Typical instrument parameters were: X-ray tube settings 50 kV and 200 μA, X-ray beam collimator diameter and reconstructed pixel size 1 mm or 0.5 mm, on-the-fly scanning acquisition with a horizontal speed of 15–25 mm/s, single spectra acquisition time 30 ms. All the X-ray datacubes were fitted with PyMCA software to generate the elemental maps.

3 Results

3.1 Characterization of different pigments

Firstly, the reference model paints were characterized in terms of lifetime and emission spectrum through TRPL spectroscopy and the PL imaging protocol. Table 1 presents a summary of the PL properties of the 13 emitting pigments among the 42 pigments

Table 1 Summary of the PL properties of the 13 emitting pigments. For each timescale investigated, we report the emission peak and its FWHM (in brackets) and the lifetime according to literature or the effective lifetime calculated by means of a nonlinear triexponential decay model

| Paint	Chemical composition	ns emission peak (FWHM) [nm]	ns emission lifetime [ns]	μs emission peak (FWHM) [nm]	μs effective lifetime [μs]
Zinc White	ZnO	380 (20)	1.5[50]	420 (50)	6
				545 (145)	8
Kremer White	$ZrSiO_4$	–	–	620 (190)	27
				575 (10)	209
				>750	629
Titanium White (Rutile)	TiO_2	–	–	820 (100)	35
Barium White	TiO_2	–	–	660 (160)	231
Lead White	$PbCO_3$	–	–	600 (80)	415*
Cadmium Red	$CdS_{1-x}Se_x$	600 (35)	ps timescale [35]	>750	13
Cadmium Yellow	$Cd_{1-x}Zn_xS$	508 (30)	ps timescale [35]	>700	42
Madder Lake	Alizarin, Purpurin	600 (150)	few ns [21, 36]	–	–
Lapis Lazuli	$Na_8(Al_6Si_6O_{24})S_n$ and accessory minerals [48]	–	–	625 & 730 (200)	12
Egyptian Blue	$CaCuSi_4O_{10}$	–	–	>850	87*
Han Blue	$BaCuSi_4O_{10}$	–	–	>850	9*

*Biexponential fit

investigated (see Table S1 in SI). Although the list of pigments analysed is not completely exhaustive, it includes most of the known luminescent pigments and the most widely used ones.

At the nanosecond timescale, only zinc white, cadmium yellow, cadmium red and madder lake pigments show an emission distinguishable from the spectrally broad emission of binding media typically used in paints. The nanosecond emission of these pigments has to be ascribed to the near-band edge (NBE) emission of ZnO- [28] and CdS- [34, 35] based pigments and π-π* type transitions in madder lake [36], respectively. It is important to note that the NBE emission of CdS-based paints is detected only when the material is excited with a sufficiently high fluence density, due to the dependence of the emission on the excitation fluence, as described in literature [35, 37]. With the laser used in the present research, this condition is achievable only if the laser beam is focused in an analysis spot no more than a few millimeters in diameter, hence during the TRPL spectroscopy analyses conducted on the model paints. Instead, in ZnO-based paints, NBE emission is detected in both imaging and spectroscopy measurements, due to the different dependence of ZnO emission on the excitation fluence [37].

At the microsecond timescale, semiconductor pigments (as zinc white [28], cadmium yellows and reds [13] and titanium white in rutile form [38]) exhibit an emission ascribed to trap energy levels present within the band gap. Egyptian and Han Blue show the well-known near-infrared microsecond emission upon excitation in Cu^{2+} d − d transitions [39]. The emission recorded following UV excitation could be due to the trapping of an exciton at a copper site yielding an excited Cu^{2+}, which then gives rise to the emission of NIR photons through the $^2B_{2g} \rightarrow {}^2B_{1g}$ transition, as recently hypothesized by Binet et al. [40]. Kremer White, based on Zirconium silicate ($ZrSiO_4$) accordingly to manufacturer's declaration, shows a broad band emission at the microsecond timescale (between 550 and 700 nm) as well as a sharp emission peak at 575 nm and a NIR band beyond 750 nm, both occurring at the millisecond timescale (see Fig. S2 in SI). These millisecond emissions can be ascribed to impurities acting as emitting centres (such as Dy^{3+}) [41, 42] or to oxides commonly present in $ZrSiO_4$ [43]. Crystalline pigments, as barium white and lead whites, present a broad emission ascribed to substitutional ions in $BaSO_4$ crystal structure [44–46] and to defects in the crystal structure of lead carbonate, although lead white pigments are excited with an energy below the optical gap (4.5–5 eV) [47]. Lastly, natural ultramarine (Lapis Lazuli) shows a microsecond emission, while its synthetic counterpart does not show any emission at the microsecond timescale. This emission is constituted by two different contributions (peaked at 625 and 730 nm) with a similar lifetime (see Fig. S3 in SI). As Lapis Lazuli usually contains lazurite along with a variety of accessory minerals as calcite, pyrite, sodalite, forsterite and muscovite [48], it is reasonable to hypothesize that the emission is due to one of these accessory materials that often show emission from impurity centres [43] and are absent in the much purer synthetic ultramarine pigment. In particular, accordingly to Gaft et al. [43], the emission at 630 nm can be related to calcite, while the emission at 725 can be related to sodalite.

It is worth noting that the PL intensity highly differs for the analysed paints. Although this parameter cannot be considered in terms of its absolute value due to the variability in concentration of pigments in paints, the different absorption of the fluorophores at the excitation wavelength ($\lambda_{exc} = 355$ nm) and their different quantum yield, it should be noted that the emission of zinc white paint occurring at the microsecond timescale is much more intense than the ones displayed by other luminescent paints. Such
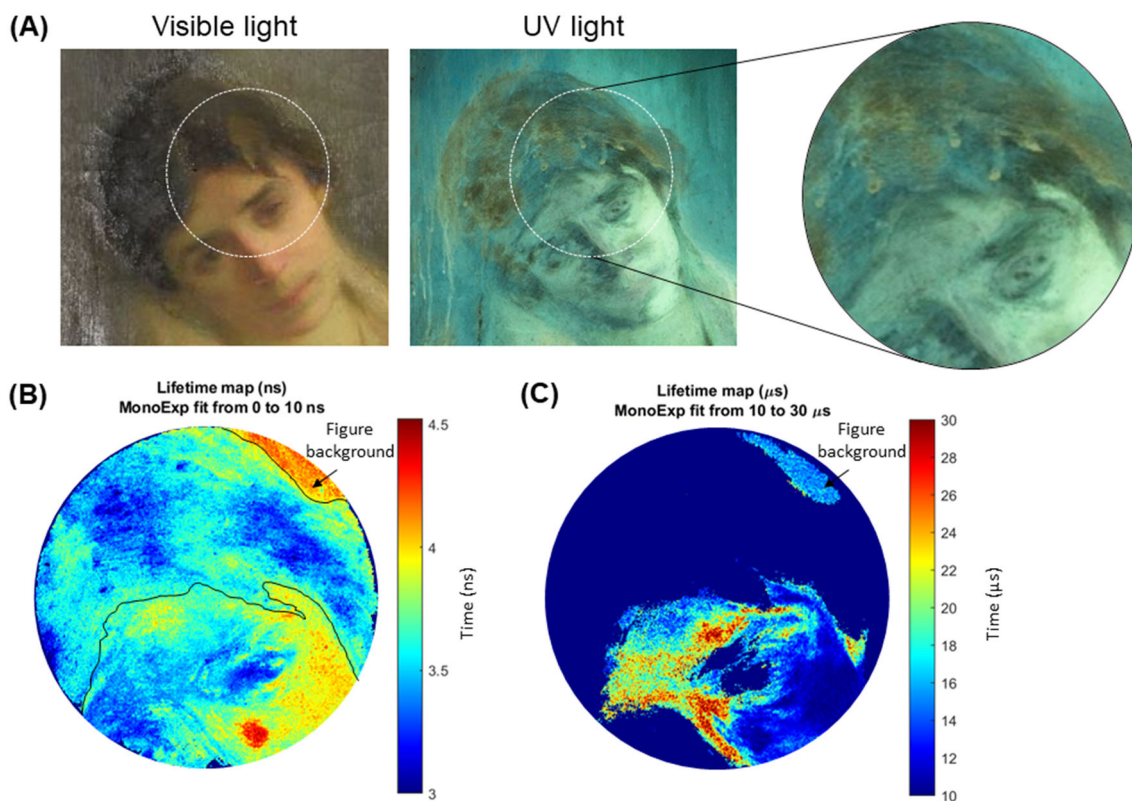
Fig. 2 A Visible and UV-excited PL image of a part of the painting *Madre* by Pietro Verzetti and selected area for luminescence lifetime imaging measurements (white circle). Lifetime measurements were performed at two different timescales: **B** nanosecond timescale (gate = 10 ns, delay from 0 to 57 ns) and **C** microsecond timescale (gate = 10 μs, delay from 10 to 100 μs). For each timescale, a false colour map of the PL lifetime is reconstructed through a mono-exponential fit, highlighting the distribution of the lifetime within the selected area of interest. In the nanosecond lifetime map (panel **B**), hair contour lines have been drawn to better highlight the different areas

intense emission can be easily detected even with steady-state imaging techniques [49] (as the simple UV photography or steady-state hyperspectral imaging) and tends to cover the emission of other compounds. Therefore, different PL imaging techniques are required to detected weaker emissions, as will be highlighted in this paper.

3.2 Case study I: Madre by Pietro Verzetti

In the painting *Madre*, the author used different materials to obtain a glossy or matt finishes to create the volume of the figure. Notably, restorers have hypothesized the use of several types of varnishes together with organic and inorganic pigments. The area of the woman's head (Fig. 2A) was analysed to map and identify the luminescent materials used for the complexion.

PL lifetime imaging was performed at two different timescales. Video datasets of the two time-decay measurements are available in SI. At both the nanosecond and microsecond timescale, the analysed portion of the painting display emission lifetimes that are spatially-heterogeneous. In particular, at the nanosecond timescale (Fig. 2B), two main lifetimes can be distinguished in the hair area, while in the left part of the woman's face and in the figure background (top right, Fig. 2B) an emission with a longer lifetime is present. Delaying the collection of the PL emission at the microsecond timescale (Fig. 2C), it is possible to observe a further uneven distribution of the lifetime in the face, with a more long lived microsecond emission in the forehead, nose bridge and left part of the nose and a shorter emission – but still occurring at the microsecond timescale–on the left cheek of the figure. Instead, no emission from the hair area is detected at the microsecond timescale.

After identifying the order of magnitude of the lifetime of the emission present in the painting, two time-gated hyperspectral datacubes were acquired to study the spectral behaviour of the emissions occurring at the nanosecond and microsecond timescales. The time-gated hyperspectral datacube recorded at the nanosecond timescale (i.e. by collecting only photons occurring in a temporal window of 100 ns synchronous with the pulsed laser excitation) allows one to reconstruct slightly different emission spectra in the hair area (see Fig. S4 in SI), with regions of the hairstyle displaying a broad band contribution shifted in the red with respect to the emission of the hairline on the forehead. At the microsecond timescale (i.e. by collecting only photons occurring in a temporal window of 10 μs delayed by 0.2 μs from pulsed excitation), we infer that the emissions detected in correspondence of the left cheek
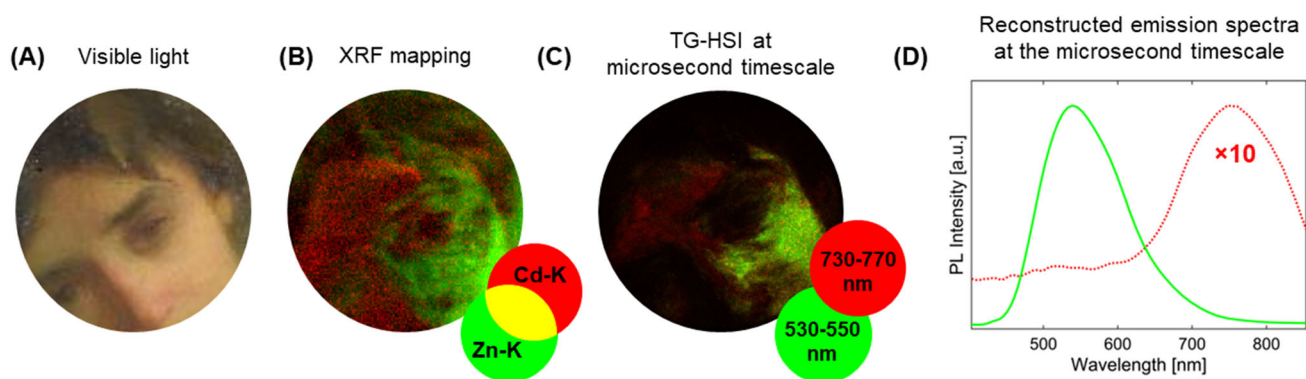
Fig. 3 **A** Visible image of the analysed area of the painting *Madre* by Pietro Verzetti. **B** Elemental maps of Zn-K and Cd-K combined in a false colour representation. **C** Composite image achieved by combining in a false colour representation the intensity images of the PL emission occurring at the microsecond timescales in two selected spectral ranges. **D** Time-gated emission spectra reconstructed in correspondence of the cheek area (green spectrum) and forehead area (red spectrum). Spectra are shown following intensity normalization at the emission peak to ease spectral comparison. We note here that the emission detected on the forehead (red spectrum) is less intense by an order of magnitude with respect to the emission detected on the left cheek (green spectrum)

and the forehead (Fig. 3D) differ also for their spectral behaviour and intensity, with the former being peaked at 540 nm, and the latter, less intense by one order of magnitude, being peaked at 750 nm.

Based on the recorded emission lifetimes and spectra, it is possible to make some assumptions on the pictorial materials used by the artist. In the area of the woman's head, painted with a brown/dark pigment, we detected a heterogeneous emission occurring only at the nanosecond timescale, an issue that is rather indicative of the presence of organic materials as the emitting species. In particular, we attribute the detected nanosecond emissions to the presence of (at least) two different varnishes characterized by different lifetime, hence accounting for the displayed lifetime heterogeneities [51]. This difference is also visible in the spectral emission. Indeed, region in the top part of the hair (with a shorter lifetime, 3 ns) has a broad band contribution shifted in the red with respect to the emission of the lower part (longer lifetime, 3.7 ns). However, it is not possible to provide any chemical identification only based on their PL emission spectra and lifetimes and other molecular techniques are required for a precise identification of the varnish types.

In the face of the figure, a microsecond emission is present, which allows us to assume the use of inorganic luminescent pigments for the complexation of the woman. On the basis of the measured lifetime and spectral behaviour of the microsecond emission, we infer the use of zinc white (emission peaked at 540 nm with a lifetime of $\sim 10\,\mu s$) on the left cheek and of cadmium yellow (emission peaked at 750 nm with a lifetime of 20–30 μs) on the forehead and right part of the face. It is worth noting that the spatial distribution of the microsecond emission (see Fig. 3C), reconstructed by combining the intensity images in the spectral regions $\pm 10/20$ nm around the emission peak, is in strong agreement with the elemental distribution of Zn and Cd identified by XRF mapping (see Fig. 3B).
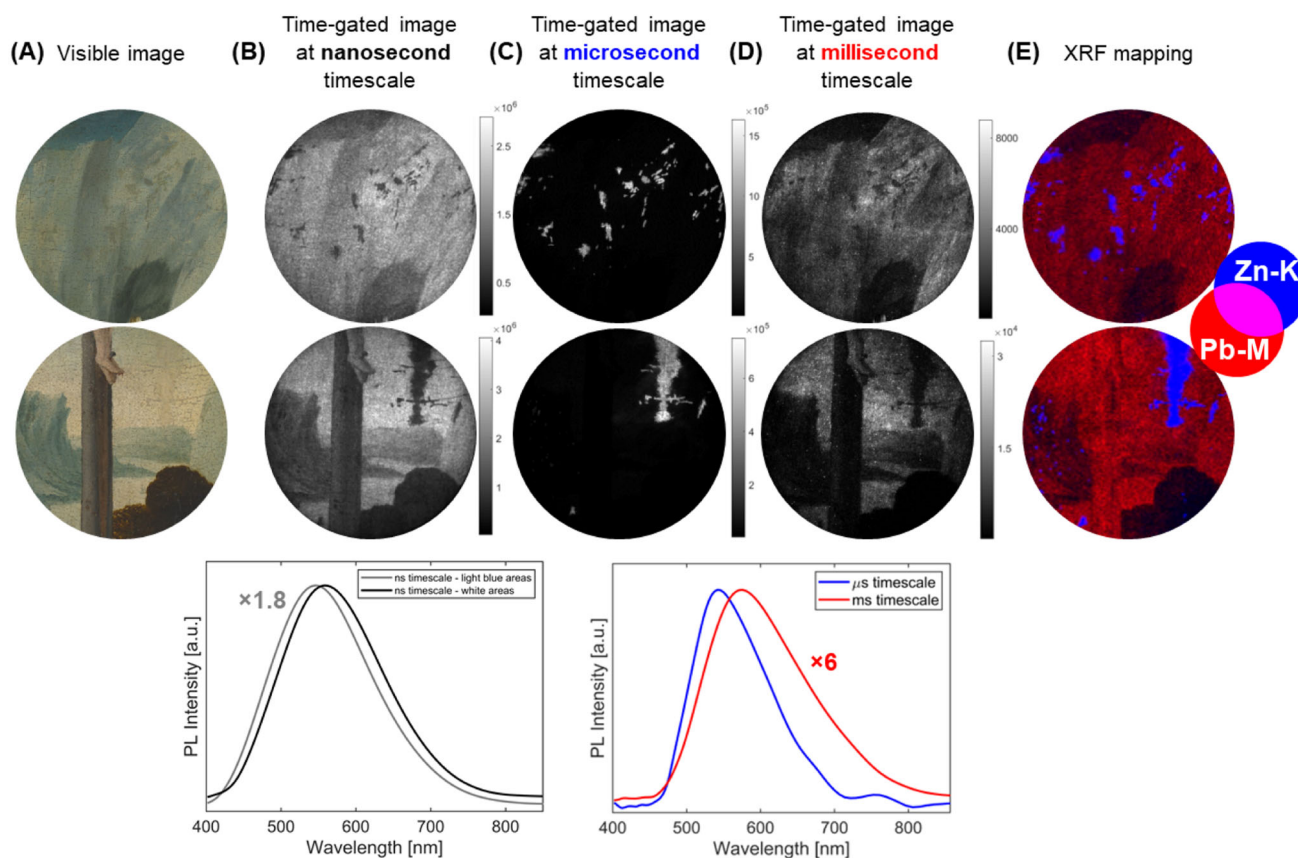
3.3 Case study II: Christ en croix et Saintes Femmes by Albrecht Altdorfer

The second case study is a Renaissance painting by Albrecht Altdorfer. The painting was analysed prior to restoration intervention to identify the pigments used, locate retouched areas and guide the restoration work. Several areas of the painting were investigated through the time-resolved imaging protocol, and we report here the most interesting results obtained on two different areas corresponding to the mountain above the cave and the landscape behind the crucifix feet (Fig. 4A).

The emission detected from painting at the nanosecond timescale does not reveal any specific and clear feature, either in terms of lifetimes (Fig. S5 in SI) or spectral behaviour (Fig. 4B, bottom), that could let us identify a specific emitting specie or to map emitting species located in specific areas of the painting. We speculate that this nanosecond emission is ascribed to the one of the varnish and/or organic binder used by the painter. Indeed, past research demonstrated that these types of organic compounds exhibit nanosecond emissions with spectral and lifetime feature that does not allow to differentiate between them [51].

At the microsecond timescale the spatial distribution of the emission drastically changes with some localized small regions displaying a well-detectable emission (Fig. 4C). This emission, with an effective lifetime of $\sim 5.8\,\mu s$ (mono-exponential fit from 0.1 to 15 μs) and spectrally peaked at 540 nm, can be ascribed to the trap state emission of zinc white-based paint. It is interesting to note that at this timescale the emission intensity decreases by an order of magnitude with respect to the one occurring at the nanosecond timescale.

Delaying further the detection towards the millisecond timescale, once the intense microsecond emission of the zinc white retouching has decayed, the spatial morphology of the emission changes again and areas painted white appear as luminescent (Fig. 4D). The emission, with an intensity decreased of two orders of magnitude with respect to the one occurring at the nanosecond

Fig. 4 A Visible image of the analysed area of the painting *Christ en croix et Saintes Femmes* by Albrecht Altdorfer. **B** Time-gated image at the nanosecond (gate 100 ns, delay 0 ns) and reconstructed mean emission spectra of selected light blue and white areas. (**C**, **D**) Time-gated image at the microsecond (gate 10 μs, delay 0.2 μs) and millisecond (gate 10 μs, delay 100 μs) timescales, and reconstructed mean emission spectra of the emitting areas at the different timescales. Colourbars in the images (**B**, **C**, **D**) shows the intensity of the emission in the whole area analysed. **E** Elemental maps of Zn-K and Pb-M combined in a false colour representation

timescale, has a lifetime of hundreds of microseconds (~500 μs, mono-exponential fit from 0.1 to 1 ms) and a broad spectral shape peaked at 580 nm. Based on the characterization performed on reference luminescent paints and by also looking at the XRF elemental maps (Fig. 4 E), we infer this millisecond emission is associated to the use of a lead white-based paint.
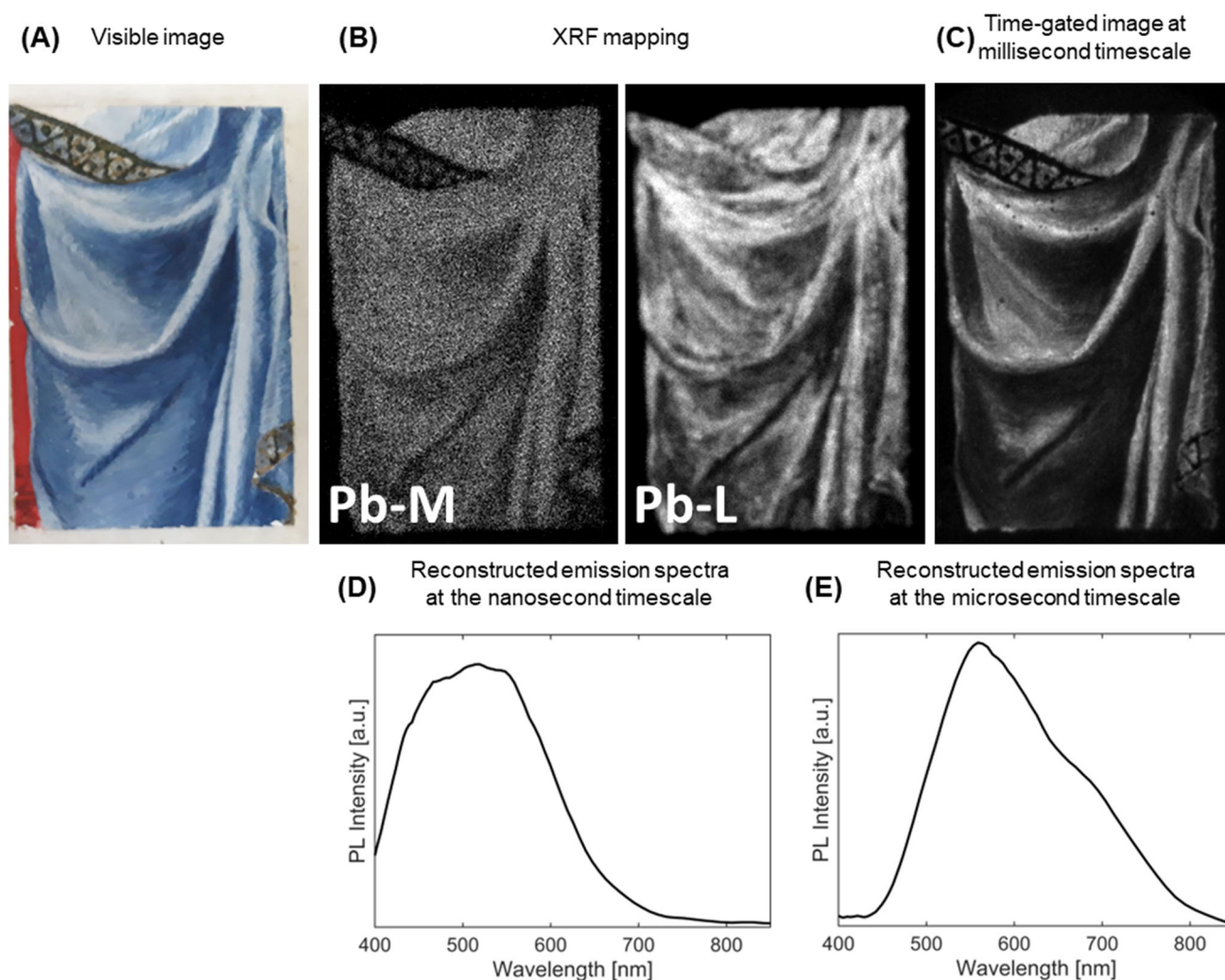
3.4 Model paint

To further demonstrate the possibility of detecting the faint emission of lead white in the presence of stronger emitting compounds, analysis on the model painting was finally performed. The painting depicts a blue draped cloth painted in lead white and synthetic ultramarine blue pigments in an egg-based binding medium. While at the nanosecond timescale, the emission detected corresponds to the broad emission of the binding medium (Fig. 5D), at the millisecond timescale, the light blue/whitish paint shows an emission with an effective lifetime of ~415 μs (mono-exponential fit from 0.1 to 1 ms), peaked at 560 nm (Fig. 5E). A shoulder at higher wavelengths (700 nm) is also present, probably ascribed to the influence of ultramarine pigments and its reabsorption effect [18]. The spatial distribution of the emission at the microsecond timescale (Fig. 5C) well matches with the XRF Pb-L map (Fig. 5B). Indeed, due to the different penetration depth of the UV radiation and X-ray, luminescence imaging measurements allow us to identify and map the use of lead white only in the superficial paint layer.

4 Discussion and conclusions

In this work, we proposed the use of combined luminescence lifetime imaging and TG-HSI to deeply characterize the luminescent materials present in paintings and assess their spatial distribution. The initial characterization of standard materials was fundamental to understand which pigments can present a luminescent emission at the different timescales. In this manner, the spectral and lifetime properties of the luminescent pigments mostly used in the Renaissance and Modern Age were assessed.

Fig. 5 A Visible image of the model paint. **B** Elemental maps of Pb-M and Pb-L lines. **C** Time-gated image at the millisecond timescale (gate 10 μs, delay 100 μs). **D** Reconstructed mean emission spectra of the light blue emitting areas at the nanosecond timescale (gate 100 ns, delay 0 ns) and **E** at the microsecond timescale (gate 10 μs, delay 1 μs)

Firstly, it is worth noting that the study only of the emission occurring at the nanosecond timescale in paintings rarely can infer a clear material identification. Indeed, at this timescale many organic materials—as varnishes, binders and colorants—emit, giving rise to luminescent signals made of the contribution of multiple emitters. Thus, even if one can accurately measure the spectral and decay behaviour of emissions, they result in the form of broad emission spectra and multi-exponential decay kinetics, which cannot be resolved into their pure components. Indeed, at this timescale, the PL imaging protocol allowed only to visualize spatial heterogeneities among the painting.

Instead, the time-resolved PL approach demonstrated to be highly effective when considering the emissions occurring at delayed times with respect to pulsed excitation. At this timescale, the method is extremely effective for the identification and mapping of weak, but long-lived luminescent compounds in artworks, thanks to the possibility of separating their emission from the one of stronger emitters. Indeed, in the painting *Madre* by Pietro Verzetti, we assessed the presence of two inorganic pigments for the complexation, namely zinc white and cadmium-based pigment, where the weaker, but longer emission of cadmium yellow paints was detected despite the presence of the overwhelming intense emission of zinc white.

A more detailed discussion is needed for lead white paints. In Altdorfer's and in the model painting, we demonstrated how it is possible to detect the faint, but long-living emission of lead white (characterized by a lifetime of hundreds of microseconds) despite the presence of other strongly luminescent materials such as varnish, binders and zinc white. It is worth noting that in Altdorfer's painting the spatial morphology of the emission occurring at the nanosecond (Fig. 4B) and microsecond (Fig. 4D) timescales and the elemental distribution achieved through XRF mapping (Fig. 4E) are similar. This may lead to associate the nanosecond emission to lead white-based paints. However, as shown by reference measurements and literature, this pigment has only a microsecond emission, associated to defects in the pigment crystal structure [47]. Therefore, the nanosecond emission must be associated to the

binder or varnish present in the painting that is absorbed by dark or coloured pigments and instead is reflected where white paints, as lead white, are present. Considering these results, particular care must be taken for the correct interpretation of the emission occurring from lead white paints when it is detected through a steady-state camera/detector. Indeed, considering that the microsecond emission from lead white paints is rather faint, we believe that its emission can be well discriminated from other strongly emitting compounds only by using a time-gated detection scheme.

The information obtained through this study allowed us to identify the luminescent materials present in the paintings analysed but also to associate them with the artist's original use and the presence of retouching or conservation interventions. Indeed, the zinc white paint found in Altdorfer's painting is associated to previous restoration treatments, due to late introduction of the material with respect to artist's activity and its localized presence. This information is extremely precious for further interventions and restoration of the artwork.

Regarding the system itself, an important upgrade will be implemented in the future by coupling the luminescence lifetime imaging system with the TG-HSI one without changing the collection objective. In this way, it will be possible to perform analysis on the same area of the painting without moving the instrument and without removing the hyperspectral interferometer within the collection path. Moreover, by coupling the system with different excitations (for example by exploiting the fourth and second harmonic of a Nd:YAG laser), the dependence of the luminescent emission from the excitation wavelength could be also exploited. In such a way, it could be possible to identify different material phases, as for example, cerussite and hydrocerussite [47].

Data Availability Statement This manuscript has associated data in a data repository. [Authors' comment: The datasets generated during and/or analysed during the current study are available from the corresponding author on reasonable request.]

Declarations

Conflict of interest The authors have no relevant financial or non-financial interests to disclose.

References

1. C. Daffara, S. Mazzocato, G. Marchioro, Multiscale roughness analysis by microprofilometry based on conoscopic holography: a new tool for treatment monitoring in highly reflective metal artworks. Eur. Phys. J. Plus. **137**, 430 (2022). https://doi.org/10.1140/epjp/s13360-022-02605-x
2. A. Dal Fovo, G.J. Tserevelakis, E. Klironomou et al., First combined application of photoacoustic and optical techniques to the study of an historical oil painting. Eur. Phys. J. Plus. **136**, 757 (2021). https://doi.org/10.1140/epjp/s13360-021-01739-8
3. V. Beltran, A. Marchetti, G. Nuyts et al., Nanoscale analysis of historical paintings by means of O-PTIR spectroscopy: the identification of the organic particles in L'Arlésienne (portrait of Madame Ginoux) by Van Gogh. Angew Chemie (2021). https://doi.org/10.1002/ange.202106058
4. M. Alunni Cardinali, L. Cartechini, M. Paolantoni et al., Microscale mechanochemical characterization of drying oil films by in situ correlative Brillouin and Raman spectroscopy. Sci. Adv. **8**, eabo4221 (2022). https://doi.org/10.1126/sciadv.abo4221
5. M. Picollo, M. Aceto, T. Vitorino, UV-Vis spectroscopy. Phys. Sci. Rev. **4**, 1–14 (2019). https://doi.org/10.1515/psr-2018-0008
6. J. Striova, A.D. Fovo, R. Fontana, Reflectance imaging spectroscopy in heritage science. Riv. Del. Nuovo. Cim. **43**, 515–566 (2020). https://doi.org/10.1007/s40766-020-00011-6
7. M. Picollo, M. Bacci, A. Casini et al., Fiber optics reflectance spectroscopy: a non-destructive technique for the analysis of works of art, in *Optical sensors and microsystems*. (Kluwer Academic Publishers, Boston, 2000), pp.259–265
8. M. Picollo, C. Cucci, A. Casini, L. Stefani, Hyper-spectral imaging technique in the cultural heritage field: new possible scenarios. Sensors (Switzerland) **20**(10), 2843 (2020). https://doi.org/10.3390/s20102843
9. F. Gabrieli, K.A. Dooley, M. Facini, J.K. Delaney, Near-UV to mid-IR reflectance imaging spectroscopy of paintings on the macroscale. Sci Advances **5**(8), eeaw7794 (2019). https://doi.org/10.1126/sciadv.aaw7794
10. J.K. Delaney, K.A. Dooley, R. Radpour, I. Kakoulli, Macroscale multimodal imaging reveals ancient painting production technology and the vogue in Greco-Roman Egypt. Sci Rep **7**, 1–12 (2017). https://doi.org/10.1038/s41598-017-15743-5
11. K.A. Dooley, A. Chieli, A. Romani et al., Molecular fluorescence imaging spectroscopy for mapping low concentrations of red lake pigments: Van Gogh's painting the olive orchard. Angew Chemie - Int Ed **59**, 6046–6053 (2020). https://doi.org/10.1002/anie.201915490
12. R. Radpour, G.A. Gates, I. Kakoulli, J.K. Delaney, Identification and mapping of ancient pigments in a Roman Egyptian funerary portrait by application of reflectance and luminescence imaging spectroscopy. Herit Sci **10**, 8 (2022). https://doi.org/10.1186/s40494-021-00639-5
13. M. Thoury, J.K. Delaney, E.R. de la Rie et al., Near-infrared luminescence of cadmium pigments. in situ identification and mapping in paintings. Appl. Spectrosc. **65**, 939–951 (2011). https://doi.org/10.1366/11-06230
14. M. Longoni, E.S. Cacciola, S. Bruni, UV-excited fluorescence as a basis for the in-situ identification of natural binders in historical painting: a critical study on model samples. Chemosensors **10**, 256 (2022). https://doi.org/10.3390/chemosensors10070256
15. Thoury M, Elias M, Frigerio JM, Barthou C Nondestructive Varnish Identification by Ultraviolet Fluorescence Spectroscopy

16. A. Dal Fovo, S. Mattana, A. Chaban et al., fluorescence lifetime phasor analysis and raman spectroscopy of pigmented organic binders and coatings used in artworks. Appl. Sci. **12**, 179 (2021). https://doi.org/10.3390/app12010179
17. A. Romani, C. Clementi, C. Miliani, G. Favaro, Fluorescence spectroscopy: a powerful technique for the noninvasive characterization of artwork. Acc. Chem. Res. **43**, 837–846 (2010). https://doi.org/10.1021/ar900291y
18. J.K. Delaney, K.A. Dooley, A. van Loon, A. Vandivere, Mapping the pigment distribution of Vermeer's Girl with a Pearl Earring. Herit. Sci. **8**, 1–16 (2020). https://doi.org/10.1186/s40494-019-0348-9
19. G. Verri, C. Clementi, D. Comelli et al., Correction of ultraviolet-induced fluorescence spectra for the examination of polychromy. Appl. Spectrosc. **62**, 1295–1302 (2008). https://doi.org/10.1366/000370208786822296
20. S. Mattana, A. Dal Fovo, J.L. Lagarto et al., Automated phasor segmentation of fluorescence lifetime imaging data for discriminating pigments and binders used in artworks. Molecules **27**, 1475 (2022). https://doi.org/10.3390/molecules27051475
21. A. Romani, C. Clementi, C. Miliani et al., Portable equipment for luminescence lifetime measurements on surfaces. Appl. Spectrosc. **62**, 1395–1399 (2008). https://doi.org/10.1366/000370208786822250
22. M. Romani, G. Capobianco, L. Pronti et al., Analytical chemistry approach in cultural heritage: the case of Vincenzo Pasqualoni's wall paintings in S. Nicola in Carcere (Rome). Microchem. J. **156**, 104920 (2020). https://doi.org/10.1016/j.microc.2020.104920
23. L. Caneve, F. Colao, R. Fantoni, L. Fiorani, Scanning lidar fluorosensor for remote diagnostic of surfaces. Nucl. Instr. Method. Phys. Res. Sect A Accel. Spectrometers, Detect. Assoc. Equip. **720**, 164–167 (2013). https://doi.org/10.1016/J.NIMA.2012.12.009
24. V. Raimondi, D. Lognoli, L. Palombi, A fluorescence lidar combining spectral, lifetime and imaging capabilities for the remote sensing of cultural heritage assets, in *Earth Res*. ed. by U. Michel, K. Schulz (Environ, Remote Sens./GIS Appl. V, 2014), pp.924597–106
25. M. Marinelli, A. Pasqualucci, M. Romani, G. Verona-Rinati, Time resolved laser induced fluorescence for characterization of binders in contemporary artworks. J. Cult. Herit. **23**, 98–105 (2017). https://doi.org/10.1016/j.culher.2016.09.005
26. M. Ghirardello, G. Valentini, L. Toniolo et al., Photoluminescence imaging of modern paintings: there is plenty of information at the microsecond timescale. Microchem. J. **154**, 104618 (2020). https://doi.org/10.1016/j.microc.2020.104618
27. D. Comelli, A. Nevin, A. Brambilla et al., On the discovery of an unusual luminescent pigment in Van Gogh's painting "Les bretonnes et le pardon de pont Aven." Appl. Phys. A **106**, 25–34 (2012). https://doi.org/10.1007/s00339-011-6665-9
28. A. Artesani, S. Bellei, V. Capogrosso et al., Photoluminescence properties of zinc white: an insight into its emission mechanisms through the study of historical artist materials. Appl. Phys. A **122**, 1053 (2016). https://doi.org/10.1007/s00339-016-0578-6
29. M. Ghirardello, C. Manzoni, M. Gironda et al., A novel photoluminescence hyperspectral camera for the study of artworks. European Phys. J. Plus **136**(10), 1052 (2021)
30. A. Nevin, A. Cesaratto, S. Bellei et al., Time-resolved photoluminescence spectroscopy and imaging: new approaches to the analysis of cultural heritage and its degradation. Sensors **14**, 6338–6355 (2014). https://doi.org/10.3390/s140406338
31. D. Comelli, C. D'Andrea, G. Valentini et al., Fluorescence lifetime imaging and spectroscopy as tools for nondestructive analysis of works of art. Appl. Opt. **43**, 2175 (2004). https://doi.org/10.1364/AO.43.002175
32. E. Ravaud, L. Pichon, E. Laval et al., Development of a versatile XRF scanner for the elemental imaging of paintworks. Appl. Phys. A **122**, 17 (2016). https://doi.org/10.1007/s00339-015-9522-4
33. R. Alberti, T. Frizzi, L. Bombelli et al., CRONO: a fast and reconfigurable macro X-ray fluorescence scanner for in-situ investigations of polychrome surfaces. X-Ray Spectrom. **46**, 297–302 (2017). https://doi.org/10.1002/xrs.2741
34. D. Anglos, M. Solomidou, I. Zergioti et al., Laser-induced fluorescence in artwork diagnostics: an application in pigment analysis. Appl. Spectrosc. **50**, 1331–1334 (1996). https://doi.org/10.1366/0003702963904863
35. A. Cesaratto, C. D'Andrea, A. Nevin et al., Analysis of cadmium-based pigments with time-resolved photoluminescence. Anal. Method **6**, 130–138 (2014). https://doi.org/10.1039/C3AY41585F
36. C. Grazia, C. Clementi, C. Miliani, A. Romani, Photochemical & photobiological sciences photophysical properties of alizarin and purpurin Al(III) complexes in solution and in solid state. Photochem. Photobiol. Sci. **10**, 1249–1254 (2011). https://doi.org/10.1039/c1pp05039g
37. M. Ghirardello, N.M. Kelly, G. Valentini et al., Photoluminescence excited at variable fluences: a novel approach for studying the emission from crystalline pigments in paints. Anal. Methods **12**, 4007–4014 (2020). https://doi.org/10.1039/D0AY01160F
38. B. van Driel, A. Artesani, K.J. van den Berg et al., New insights into the complex photoluminescence behaviour of titanium white pigments. Dye Pigment **155**, 14–22 (2018). https://doi.org/10.1016/j.dyepig.2018.03.012
39. G. Pozza, D. Ajò, G. Chiari et al., Photoluminescence of the inorganic pigments Egyptian blue, Han blue and Han purple. J. Cult. Herit. **1**, 393–398 (2000). https://doi.org/10.1016/S1296-2074(00)01095-5
40. L. Binet, J. Lizion, S. Bertaina, D. Gourier, Magnetic and new optical properties in the UV−visible Range of the Egyptian Blue Pigment Cuprorivaite $CaCuSi_4O_{10}$. J. Phys. Chem. C **125**, 25189–25196 (2021). https://doi.org/10.1021/acs.jpcc.1c06060
41. H. Friis, A.A. Finch, C.T. Williams, J.M. Hanchar, Photoluminescence of zircon ($ZrSiO_4$) doped with REE3+ (REE = Pr, Sm, Eu, Gd, Dy, Ho, Er). Phys. Chem. Miner. **37**, 333–342 (2010). https://doi.org/10.1007/s00269-009-0336-9
42. M. Gaft, G. Panczer, R. Reisfeld, I. Shinno, Laser-induced luminescence of rare-earth elements in natural zircon. J. Alloys Compd. **300–301**, 267–274 (2000). https://doi.org/10.1016/S0925-8388(99)00781-1
43. Gaft M, Reisfeld R, Panczer G (2015) Modern Luminescence Spectroscopy of Minerals and Materials. Springer International Publishing
44. M. Gaft, R. Reisfeld, G. Panczer et al., Luminescence of Bi, Ag and Cu in natural and synthetic barite $BaSO_4$. Opt. Mater. (Amst) **16**, 279–290 (2001). https://doi.org/10.1016/S0925-3467(00)00088-4
45. M. Gaft, I. Rudenkova, Laser-induced luminescence of barite after thermal treatment. J. Therm. Anal. **42**, 187–195 (1993)
46. A.S. Marfunin, *Spectroscopy* (Luminescence and Radiation Centers in Minerals, Springer, Berlin Heidelberg, Berlin, Heidelberg, 1979)
47. V. Gonzalez, D. Gourier, T. Calligaro et al., Revealing the origin and history of lead-white pigments by their photoluminescence properties. Anal. Chem. **89**, 2909–2918 (2017). https://doi.org/10.1021/acs.analchem.6b04195
48. C.M. Schmidt, M.S. Walton, K. Trentelman, Characterization of lapis lazuli pigments using a multitechnique analytical approach: Implications for identification and geological provenancing. Anal. Chem. **81**, 8513–8518 (2009). https://doi.org/10.1021/ac901436g
49. E.R. de la Rie, Fluorescence of paint and varnish layers (Part 1). Stud. Conserv. **27**, 1–7 (1982). https://doi.org/10.1179/sic.1982.27.1.1
50. A. Artesani, F. Gherardi, A. Nevin et al., A photoluminescence study of the changes induced in the Zinc white pigment by formation of zinc complexes. Materials (Basel) **10**, 340 (2017). https://doi.org/10.3390/ma10040340
51. A. Nevin, G. Spoto, D. Anglos, Laser spectroscopies for elemental and molecular analysis in art and archaeology. Appl. Phys. A **106**, 339–361 (2012). https://doi.org/10.1007/s00339-011-6699-z